Journal of Atmospheric and Solar-Terrestrial Physics 172 (2018) 100–106

Contents lists available at ScienceDirect

Journal of Atmospheric and Solar-Terrestrial Physics

journal homepage: www.elsevier.com/locate/jastp

Research Paper

Propagation of non-stationary acoustic-gravity waves at thermospheric temperatures corresponding to different solar activity

N.M. Gavrilov [a,*], S.P. Kshevetskii [b], A.V. Koval [a]

[a] Atmospheric Physics Department, Saint-Petersburg State University, Saint-Petersburg, Russia
[b] Theoretical Physics Department, Immanuel Kant Baltic Federal University, Kaliningrad, Russia

ARTICLE INFO

Keywords:
Acoustic-gravity waves
Solar activity
Thermosphere
Wave propagation
Numerical simulation
Wave-induced jets

ABSTRACT

Numerical simulation of non-stationary nonlinear acoustic-gravity waves (AGWs) propagating from the surface wave source to the thermosphere reveals that their propagation conditions and parameters depend on changes in background temperature, density, composition, molecular viscosity and heat conduction caused by changes in solar activity (SA). At small wave source amplitudes, AGW amplitudes, momentum fluxes and wave accelerations of the mean flow are slightly larger at altitudes about 150 km at low SA because of smaller mean density and $\rho_0^{-1/2}$dependence of wave amplitudes at low dissipation. Larger kinematic coefficients of molecular viscosity and heat conduction lead to stronger decrease of wave amplitudes and momentum fluxes at altitudes above 150 km at low SA. At large amplitudes of surface wave excitation, AGW breaking and smaller-scale inhomogeneities appear at altitudes 100–150 km, which are stronger at low SA. Increased dissipation of breaking AGWs may produce wave-induced jet streams with velocities close to the wave horizontal phase speed and near-critical layers at altitudes 110–150 km, which dramatically decrease amplitudes and momentum fluxes of the primary AGW mode propagating from the surface wave source. The wave-induced horizontal wind becomes smaller above altitude of 150 km and allows growing amplitudes of the primary wave mode partially penetrating through the near-critical layer and of secondary AGW modes, possibly generating in the wave induced jet stream. The wave amplitude grows at altitudes higher than 150 km is larger at high SA due to smaller velocities of wave-induced mean wind and smaller molecular viscosity and heat conduction. Accelerations of the mean flow by dissipating AGWs are generally larger at low SA. This determines faster grows of wave-induced jet streams in time at low SA. In almost all simulated cases, velocities of the wave-induced mean flows are higher at low SA compared to high SA. Resulting SA impact at a given thermospheric altitude depends on competition between AGW amplitude increase due to smaller molecular dissipation and smaller energy transfer to the wind-induced mean flow and amplitude decrease caused by larger density and stronger reflection at higher SA.

1. Introduction

Numerous studies show that acoustic-gravity waves (AGWs) continuously exist in the middle atmosphere (e.g., Fritts and Alexander, 2003). Observations frequently detect AGW presence in the thermosphere (e.g., Djuth et al., 2004; Park et al., 2014; Yue et al., 2010). Modeling atmospheric general circulation demonstrated that AGWs can propagate from the lower atmosphere to the thermosphere in the Earth's atmosphere (e.g., Yiğit et al., 2014; Yiğit and Medvedev, 2009, 2012, 2015) and at other planets (Yiğit et al., 2015a; Yiğit and Medvedev, 2016, 2017).

AGWs are frequently studied with non-hydrostatic numerical models. Baker and Schubert (2000) simulated nonlinear AGWs in the atmosphere of Venus. Some studies (Andreassen et al., 1998; Fritts and Garten, 1996; Fritts et al., 2009, 2011) used two-dimension modeling of wave breaking, turbulence generating and Kelvin-Helmholtz instabilities in the atmosphere. They exploit three-dimensional simulations of AGWs and turbulence in atmospheric regions with fixed vertical and horizontal sizes. These numerical algorithms made use of Galerkin-type series to alter partial differential equations to the ordinary equations for the coefficients of the spectral series. Liu et al. (2009) modeled propagation of AGWs and generation of Kelvin-Helmholtz vortexes in the mesopause region. Yu and Hickey (2007) and Liu et al. (2008) have applied two-dimensional numerical models to describe atmospheric AGW propagation.

* Corresponding author.
E-mail address: n.gavrilov@spbu.ru (N.M. Gavrilov).

https://doi.org/10.1016/j.jastp.2018.03.021
Received 10 December 2017; Received in revised form 26 March 2018; Accepted 28 March 2018
Available online 30 March 2018

AGWs coming from the troposphere to the thermosphere were simulated in general circulation models (e.g., Yiğit et al., 2012a, 2014) with a state of the art whole atmosphere gravity wave parameterization of thermal and dynamical impacts of dissipating and saturated atmospheric waves (Yiğit et al., 2008). This nonlinear scheme alleviates the majority of the weaknesses of ad hoc linear GW schemes and it especially removes the necessity of any tuning parameters. Applications of this scheme to a Martian general circulation model (GCM) has demonstrated that tropospheric GWs can propagate into the thermosphere (Medvedev et al., 2013; Yiğit et al., 2015a). More recently, the whole atmosphere scheme has successfully been used to interpret Martian thermospheric GWs observed by the MAVEN spacecraft (Yiğit et al., 2015b).

AGWs can propagate from below, break and generate turbulence in the middle and upper atmosphere. Tropospheric mesoscale turbulence and convection may generate AGWs (e.g., Fritts and Alexander, 2003; Fritts et al., 2006). Turbulent wave sources can be more extensive in tropospheric jet streams, which have maxima in the upper troposphere (e.g., Medvedev and Gavrilov, 1995; Gavrilov and Fukao, 1999; Gavrilov, 2007). Non-hydrostatic models of the general circulation of thermosphere-ionosphere revealed that AGWs constantly exist in the thermosphere (e.g. Yiğit et al., 2012b).

Gavrilov and Kshevetskii (2013a) simulated nonlinear AGWs using a two-dimensional numerical model involving basic conservation laws. This numerical model allowed non-smooth solutions of equations of nonlinear AGWs and provided the needed numerical stability (Kshevetskii and Gavrilov, 2005). A three-dimensional version of this algorithm was build up by Gavrilov and Kshevetskii (2013b, 2014a) for simulating atmospheric nonlinear AGWs. The authors modeled AGWs excited by monochromatic horizontally homogeneous wave source at the ground. Karpov and Kshevetskii (2014) used the same numerical scheme for simulating infrasound propagation from non-stationary localized surface wave sources and found substantial infrasound thermal effects in the thermosphere. Dissipating AGWs can be also responsible for wave accelerating the mean flow in the upper atmosphere (e.g., Fritts and Alexander, 2003). However, peculiarities of the mean flows and thermal effects produced by non-stationary nonlinear atmospheric AGWs require further elucidations.

There are many evidences of the influence of solar activity (SA) on AGW characteristics in the thermosphere (e.g., Gavrilov, 1995; Klausner et al., 2009; Yiğit and Medvedev, 2010). SA changes the absorption of solar radiation producing changes in the thermospheric temperature and related changes in the density, static stability and dissipation, which can alter AGW propagation conditions. Differences of AGW characteristics in relatively cold and hot thermosphere were analyzed previously (e.g., Hickey, 1987; Yiğit and Medvedev, 2010). Numerical simulations of AGW propagation to the thermosphere from tropospheric convective sources at temperature profiles for different solar activity (Vadas and Fritts, 2006; Vadas, 2007; Fritts and Vadas, 2008) demonstrated better AGW propagation at high SA due to reduced dissipation. However, increased AGW reflection caused by larger temperature gradients can compete with enhanced propagation. These conclusions are in agreement with earlier studies (Francis, 1973; Richmond, 1978; Gavrilov et al., 1994).

In the present study, with the computational model developed in the works by Gavrilov and Kshevetskii (2013b, 2014a), we simulate nonlinear AGWs propagating from non-stationary wave source, located on Earth's surface, into the thermosphere using vertical profiles of background temperature, density, molecular weight, kinematic molecular viscosity and heat conduction characteristic for different SA levels. We applied simple AGW sources corresponding to plane wave spectral components of surface vertical velocity and compared wave characteristics and wave thermal and dynamical effects at different thermospheric altitudes at low and high SA levels. Nonlinear model involves wave-wave and wave-mean flow interactions, which lead to the energy transfer from primary AGW to secondary waves and to the mean flow. Differences in these processes at different SA levels can change AGW characteristics in the middle and upper atmosphere in addition to changes in wave dissipation and reflection processes.

2. Numerical model

In the present paper, we used the three-dimensional high-resolution AtmoSym model simulating atmospheric AGWs, which was developed by Gavrilov and Kshevetskii (2013a,b, 2014a,b,c). Recently this model becomes available for free online simulations for all users (AtmoSym, 2016). The AtmoSym is a three-dimensional high-resolution model and uses the plain geometry. The model calculates atmospheric velocity components and deviations of temperature, pressure, and density from their background values. Used in AtmoSym nonlinear three-dimensional primitive equations (Gavrilov and Kshevetskii, 2013a,b; 2014a) of continuity, motion and heat balance take into account nonlinear and dissipative processes accompanying wave propagation. They can describe, in particular, such complex phenomena as wave breaking and turbulence generation (e.g., Kshevetskii and Gavrilov, 2005).

The AtmoSym numerical model provides a self-consistent description of wave processes and takes into account the changes in atmospheric parameters due to energy transfer from decaying waves to the atmosphere. Vertical profile of the background temperature $T_0(z)$ is taken from the semi-empirical atmospheric models NRLMSISE-00 (Picone et al., 2002). Background molecular dynamic viscosity, η_0, and heat conductivity, κ_0, are approximated with the Sutherlands formula

$$\eta_0 = \frac{1.46\times 10^{-6}\sqrt{T_0}}{1+110/T_0}\quad \left(\frac{kg}{m\cdot s}\right)$$
$$\kappa_0 = \frac{\eta_0}{\mathrm{Pr}_m};\quad \mathrm{Pr}_m = \frac{4\gamma}{9\gamma-5}, \tag{1}$$

where T is temperature, Pr_m is the molecular Prandtl number, γ is the ratio of air heat capacities at constant pressure and volume (Kikoin, 1976). The AtmoSym also takes into account vertical profiles of the background turbulent viscosity and thermal conductivity with maxima about 10 m^2s^{-1} near the ground and at altitude of 100 km, and a minimum of 0.1 m^2s^{-1} in the stratosphere (Gavrilov and Kshevetskii, 2013a,b; 2014a).

At the upper boundary $z \approx 600$ km, we assume zero vertical velocity and zero vertical gradients of the other wave parameters (Gavrilov and Kshevetskii, 2014a; b; c). These conditions can produce reflections of waves propagating from below. Our estimations show that such reflected waves become negligible below 400–450 km due to high dissipation and density increase. In the present research, we made calculations in a three-dimension region of the atmosphere and assume horizontal periodicity of wave source and solutions at horizontal boundaries (see Gavrilov and Kshevetskii, 2014a). At the lower boundary (the Earth's surface), we assume zero horizontal velocity and zero vertical gradients of temperature, density and pressure. For the wave excitation at the lower boundary, we assume horizontally periodical distributions of vertical velocity at the Earth's surface in the form of

$$w_{z=0} = W_0 \cos\left(\sigma t - \vec{k}\cdot\vec{s}\right), \tag{2}$$

where σ is frequency, $\vec{s} = (x_1, x_2)$is radius-vector in horizontal plane, $\vec{k} = (k_1, k_2)$ is horizontal wave number and k_1 and k_2 are wavenumbers along the horizontal axes x_1 and x_2, respectively; W_0 is the surface amplitude of the considered wave mode. The plane wave excitation (2) can approximate spectral components of turbulent and convective AGW sources (Townsend, 1965, 1966). Studies of AGW generation by meteorological and turbulent processes in the atmosphere (e.g. Medvedev and Gavrilov, 1995) showed a broad variety of periods, wavelengths, amplitudes and other wave parameters.

Solar activity produces substantial changes in the background fields, which influence AGW propagation in the middle and upper atmosphere.

In the NRLMSISE-00 model, the SA influence is specified by changes in the solar flux $F_{10.7}$ of radio waves with length of 10.7 cm (Picone et al., 2002). Fig. 1 shows vertical profiles of January background temperature, T_0, density, ρ_0, kinematic viscosity, ν, and molecular weight of atmospheric air μ for values of $F_{10.7} = 70$, 120, 250 sfu corresponding to the low, medium and high SA, respectively. One can see that T_0, ρ_0, μ are substantially smaller and ν is larger in the thermosphere at low SA compared to high SA level. Influences of these changes on AGW propagation are analyzed below.

Our numerical simulations starts from non-perturbed steady state atmosphere with zero wind and background profiles of T_0,ρ_0, μ and ν corresponding to January and different SA shown in Fig. 1. Simulations were made for the surface wave forcing (1) with varying amplitudes $W_0 \sim$ 0.1–1 mm/s, horizontal phase speeds $c_x \sim$ 30–100 m/s and period $\tau = 2 \times 10^3$ s.

Previous simulations with the AtmoSym (Gavrilov and Kshevetskii, 2014a,b,c, 2015) showed that activating the surface plane wave forcing (1) generates an initial AGW pulse, which in 5–10 min reaches altitudes 100–200 km and above. To make the source activation smoother, the forcing (1) was multiplied at times t t_0 by factor

$$r(t) = \begin{cases} \exp\left[-(t-t_0)^2/d^2\right] & at \quad t \le t_0 \\ 1 & at \quad t > t_0, \end{cases} \qquad (3)$$

where t_0 and d are constants. In the present simulations, parameters of (3) were varied within the range of $t_0 \sim$ 1–10^3 s with $d = t_0/3$.

3. Results of numerical simulations

We performed numerical simulations of nonlinear AGW propagation to the middle and upper atmosphere from a plane wave forcing at the Earth's surface (1) with period $\tau = 2 \times 10^3$ s. After activating the surface wave forcing at $t = 0$, initial pulse of acoustic and very long gravity modes in a few minutes can reach high altitudes above 100 km (Gavrilov and Kshevetskii, 2014b; c).

After dispersion and dissipation of this initial pulse, more slow internal gravity waves (IGWs) corresponding to low-frequency surface wave source (1) propagate to the upper atmosphere (Gavrilov and Kshevetskii (2015). Fig. 2 illustrates distributions of the wave vertical velocity in the vertical plane with horizontal x-axis directed along the horizontal wave vector $\vec{k}$ at $t \approx 5$ h for different solar $F_{10.7}$ flux and different amplitudes W_0 of the surface wave source (1) for sharp wave

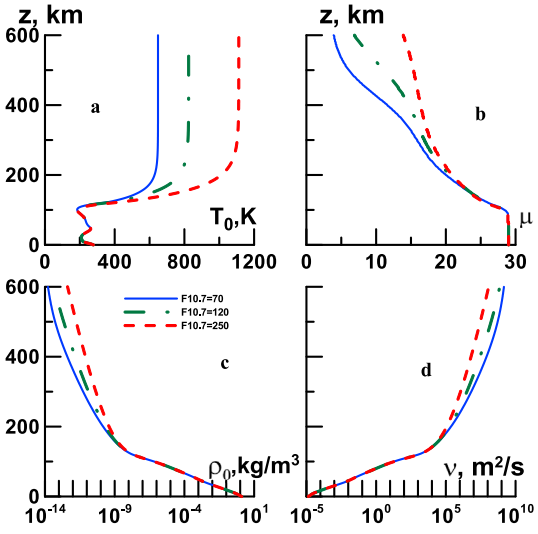

Fig. 1. Background temperature (a), molecular weight (b), density (c) and kinematic viscosity (d) for different values of solar $F_{10.7}$ radiowave flux according to the NRLMSISE-00 model.

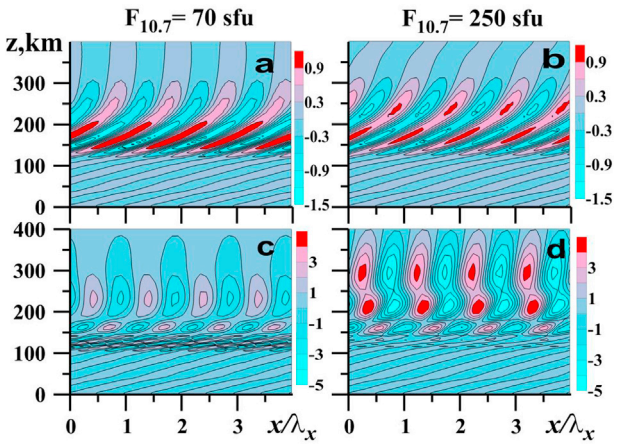

Fig. 2. . Distributions of vertical velocity (in m/s) in the plane XOZ with the axis x directed along the horizontal wave vector $\vec{k}$ at time $t = 9\tau$ for values of solar radiowave flux $F_{10.7} = 70$ sfu (left) and $F_{10.7} = 250$ sfu (right) at the amplitudes $W_0 = 0.1$ mm/s (a,b) and $W_0 = 1$ mm/s (c,d), period $\tau = 2 \times 10^3$ s and $c_x = 100$ m/s of the surface wave source (1) and interval of wave activation $t_0 = 1$ s in (3).

source activation with $t_0 = 1$s in (3). At altitudes below 100 km, one can see wave fronts inclined to the horizon, which should correspond to IGW modes propagating in the atmosphere (Gossard and Hooke, 1975). In the thermosphere, angles of the wave fronts to the horizon in Fig. 2 become larger due to influence of increased molecular viscosity and heat conductivity.

Comparison of Fig. 2a and 2c for amplitudes of the wave source (1) $W_0 = 0.1$ mm/s and $W_0 = 1$ mm/s shows the layer of small-scale inhomogeneities at altitudes 100–150 km in Fig. 2c. This can be explained by dynamical and convective instabilities of high-amplitudes IGWs at these altitudes (e.g., Gavrilov and Kshevetskii, 2015). One can see that this instability and small-scale inhomogeneities at altitudes 100–150 km are larger at low SA in Fig. 2c compared to Fig. 2d for larger value of $F_{10.7}$. Previous simulation by Gavrilov and Kshevetskii (2014b,c, 2015) showed that IGW breaking could lead to generating jet streams with the mean wind velocity up to the wave horizontal phase speed c_x. Increased wave dissipation and energy transition from the wave to the mean flow may lead to a decrease in IGW amplitudes at higher altitudes. Ratios of wave amplitudes shown in Fig. 2c and d to the respective amplitudes in Fig. 2a and b are substantially smaller (see Table 1 below) than the ratio 10 of respective amplitudes of the surface wave source (1).

Fig. 3 reveals vertical profiles of horizontal velocity at time $t \approx 30$ h for different phases varying along the horizontal x-axis during one wave period. Individual profiles overlap and produce shaded areas in Fig. 3, which show ranges of wave perturbations at each altitude. Gavrilov and Kshevetskii (2015) showed that substantial wave accelerations during the passage of initial AGW pulse may generate substantial mean

Table 1
Ratio of wave characteristics for amplitudes of the surface wave source (1) $W_{01} = 0.1$ mm/s and $W_{02} = 1$ mm/s and at different altitudes and levels of solar activity.

Parameter	$\delta w_2/\delta w_1$	$\lvert F_{m2}/F_{m1}\rvert$	$\lvert a_{wx2}/a_{wx1}\rvert$	$\lvert u_{02}/u_{01}\rvert$
Low solar activity $F_{10.7} = 70$ sfu				
$z = 100$ km	3.7	40.7	11.9	49
$z = 150$ km	0.1	0.01	0.01	8
$z = 200$ km	0.9	0.5	0.3	7
$z = 250$ km	1.0	1.3	0.9	7
High solar activity $F_{10.7} = 250$ sfu				
$z = 100$ km	2.0	9.4	3.6	69
$z = 150$ km	0.2	0.02	0.02	11
$z = 200$ km	0.9	0.1	0.2	9
$z = 250$ km	1.9	0.8	0.1	9

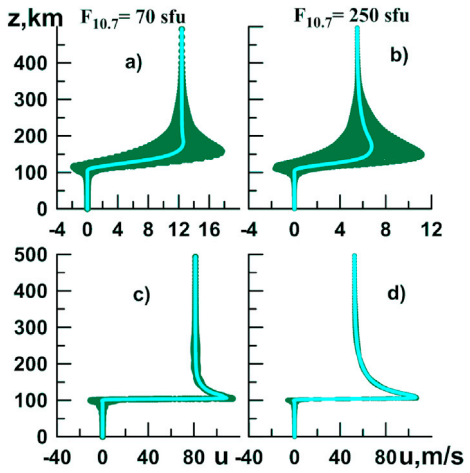

Fig. 3. Vertical profiles of the horizontal velocity perturbations produced by AGW source (1) with period $\tau = 2 \times 10^3$ s and $c_x = 100$ m/s and amplitudes $W_0 = 0.1$ mm/s (a,b) and $W_0 = 1$ mm/s (c,d) at time $t = 55\tau$ for values of solar radiowave flux $F_{10.7} = 70$ sfu (left) and $F_{10.7} = 250$ sfu (right). Thick lines show average values for each altitude.

horizontal speeds above 100 km altitudes, which exists at later times and are seen in Fig. 3.

Fig. 4 reveals similar ranges of wave perturbations of vertical velocity, which give information about wave amplitudes at different altitudes. At smaller wave source amplitude $W_0 = 0.1$ mm/s in Fig. 4a and b, the amplitudes of vertical velocity perturbations are maximum at altitudes around 150 km, and they are slightly higher in Fig. 4a for low SA. This may be explained by smaller density at those heights at low SA (see Fig. 1c). According to AGW theory (e.g., Gossard and Hooke, 1975) amplitudes of nondissipative AGWs in the lower and middle atmosphere should be proportional to $\rho_0^{-1/2}$and smaller background density corresponds to larger wave amplitude for the same wave source. Increasing molecular viscosity and heat conduction lead to decreasing wave amplitudes at altitudes above 150 km in Fig. 4a and b. Kinematic coefficients of molecular viscosity and heat conduction in Fig. 1d as well as wave dissipation rate are larger at low SA.

At larger surface wave source amplitude $W_0 = 1$ mm/s in Fig. 4c and d, the wave vertical velocity amplitudes at altitudes about 100 km are much larger than those in Fig. 4a and b, respectively. Instability and breaking these strong waves may produce jet streams (Gavrilov and Kshevetskii, 2015), which are shown with thick lines in Fig. 3c and d and may have velocity close to the horizontal phase speed of the wave source

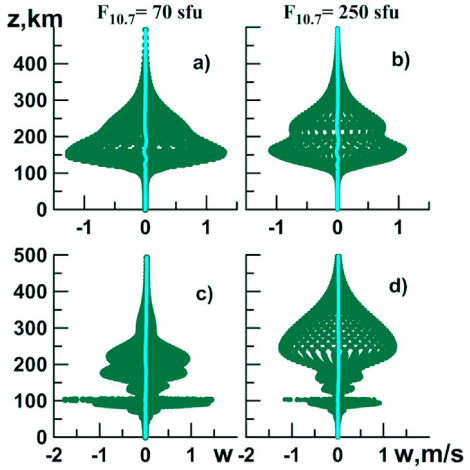

Fig. 4. Same as Fig. 3, but for vertical velocity perturbations.

(1). These jet streams can produce near-critical layer for primary wave mode propagating from the surface source, where its vertical wavelength decreases and strong dissipation of wave energy occur (e.g., Gossard and Hooke, 1975). This dissipation dramatically decreases wave amplitudes at altitudes 110–150 km in Fig. 4c and d. The wave-induced horizontal wind becomes smaller above altitude of 150 km in Fig. 3c and d, which allows growing amplitudes of the primary wave mode partially penetrating through the near-critical layer. This wave amplitude grows at $z > 150$ km is larger in Fig. 4d due to smaller molecular viscosity and heat conduction at high SA (see Fig. 1d).

Time variations of standard deviations of vertical velocity δw (which is proportional to AGW amplitude) at different altitudes are given in Fig. 5. The left panels of Fig. 5 for smaller wave source amplitude show quasi-stationary wave regimes at all altitudes after arrival IGW mode corresponding to the surface source (1) to the respective altitude. Time of this arrival is larger for higher altitude (see Gavrilov and Kshevetskii, 2014c, 2015). At altitudes 100–200 km in the left panels of Fig. 5, the δw values are larger for low SA due to smaller background density in Fig. 1c and respectively lager AGW amplitude grows due to density decrease at low dissipation (see above). Increase in molecular viscosity and heat conduction at high altitudes (see Fig. 1d) produces larger AGW dissipation at low SA and differences between δw at altitudes 200–250 km in the left panels of Fig. 5 for different SA levels become smaller.

Increases in the speed of wave-induced jet stream shown in Fig. 3a and b leads to decreases in vertical wavelength and to larger wave dissipation at altitudes above 100 km. Therefore, δw values in the left panels of Fig. 5 for smaller amplitudes of the surface wave source (1) are slightly decreasing in time. At higher amplitude of the wave source, wave-induced jet streams can reach velocities close the AGW horizontal phase speed and produce near-critical layers with strong wave dissipation (see Fig. 3c and d). This almost prevents AGW propagation, and substantially decreases δw in the right panels of Fig. 5 at altitudes higher than 100 km (see also Fig. 4c and d).

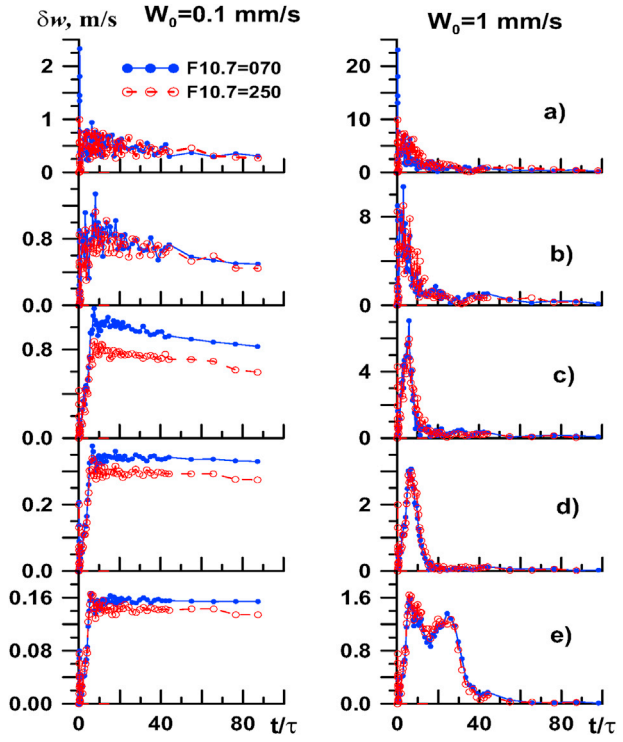

Fig. 5. Time variations of simulated standard deviation of vertical velocity at altitudes 250 km (a), 200 km (b), 150 km (c), 120 km (d), 110 km (e) for amplitudes $W_0 = 0.1$ mm/s (left) and $W_0 = 1$ mm/s (right) of the surface wave forcing (1) with period $\tau = 2{\cdot}10^3$ s and $c_x = 100$ m/s at low ($F_{10.7} = 70$ sfu) and high ($F_{10.7} = 250$ sru) levels of solar activity.

Fig. 6 demonstrates time variations of vertical wave flux of horizontal momentum $F_m = \rho_0 u'w' >$ at different altitudes (where primes and sign <> denote wave components and averaging over wave period, respectively). Time variations of F_m are similar to the time variations of wave amplitudes in Fig. 5. At smaller amplitude of the surface wave source (1) in the left panels of Fig. 6 at altitudes below 150 km, values of F_m are larger at low SA, due to the same reasons as larger AGW amplitudes at the respective left panels of Fig. 5. Wave momentum fluxes at altitudes 200–250 km in the left panels of Fig. 6, are substantially smaller at low SA, because wave amplitudes in the respective panels of Fig. 5 are close at low and high SA, but ρ_0 at low SA is much smaller, than that at high SA in Fig. 1c. In the right panels of Fig. 6 for larger wave source amplitude, wave momentum fluxes at altitudes above 100 km reach maxima at $t \sim (5–10)\tau$, when wave-induced jet streams are not so strong. After that, F_m values are substantially decreasing due to strong dissipation of the primary AGW modes in the near-critical layers formed by the wave-induced jet streams (see above).

Vertical gradients of the wave momentum flux determine the accelerations of the mean flow by AGWs $a_{wx} = -\rho_0^{-1}\partial(\rho_0 < u'w' >)/\partial z$. Fig. 7 reveals time variations of simulated wave accelerations at different altitudes for different SA levels. General behavior of wave acceleration in different panels of Fig. 7 is similar to the respective panels of Fig. 5. The a_{wx} values in Fig. 7 are generally larger at low SA. This determines faster grows of wave-induced jet streams at low SA, as it is illustrated by Fig. 8 representing time variations of the mean horizontal velocity induced by dissipating AGWs. In almost all cases shown in Fig. 7, velocities of the wave-induced mean flows are higher at low SA compared to high SA.

4. Discussion and conclusion

Simulations described above were made for the amplitudes of the surface wave source (1) $W_{01} = 0.1$ mm/s and $W_{02} = 1$ mm/s. In the linear wave model one should expect that wave amplitudes at all altitudes

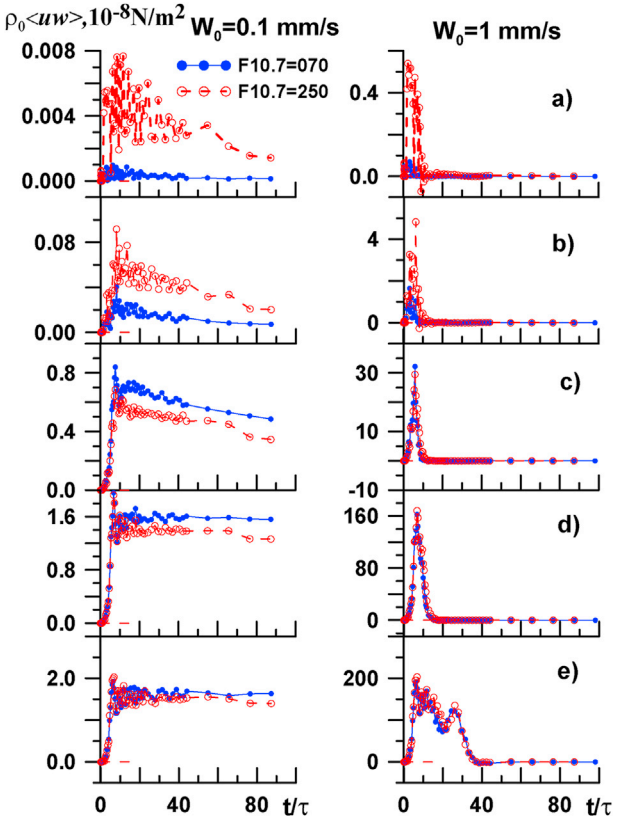

Fig. 6. Same as Fig. 5, but for the vertical wave flux of horizontal momentum.

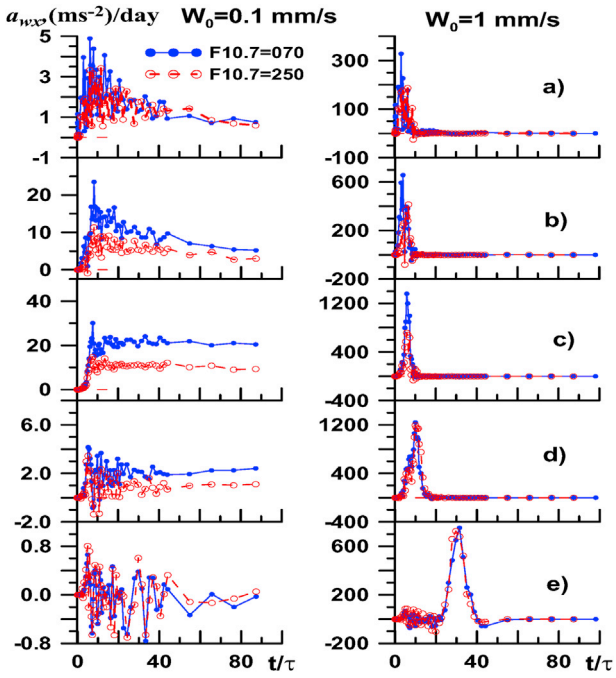

Fig. 7. Same as Fig. 5, but for the wave acceleration of the mean flow.

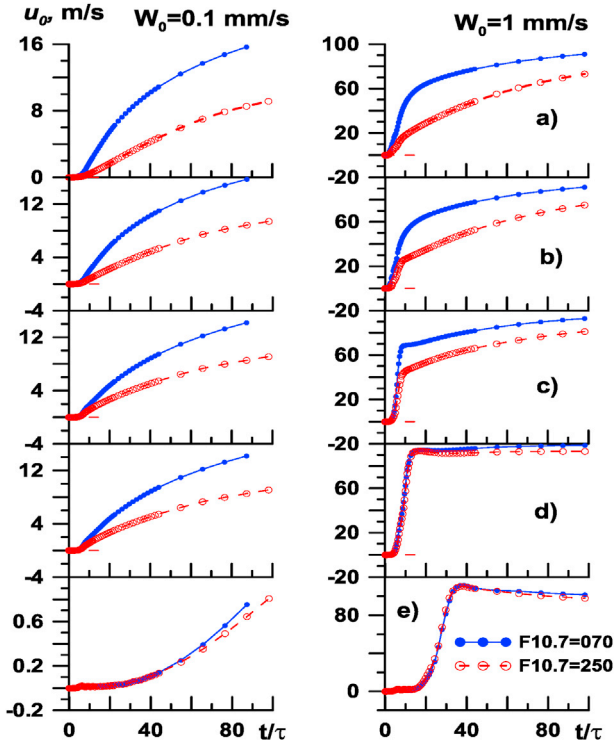

Fig. 8. Same as Fig. 5, but for the velocity of wave-induced horizontal mean flow.

should be proportional to the wave source amplitude. Nonlinear model involve wave breaking, wave-wave and wave-mean flow interactions during which the energy of primary AGW generated by the wave source can be transferred to the energy of wave-induced mean flow, turbulence and secondary AGWs. These processes are more intensive at larger amplitudes of the surface wave source (1), which may cause relatively larger loss of energy of high-amplitude AGWs. Table 1 shows ratio of wave amplitudes, momentum flux, wave accelerations and wave-induced

mean velocity for the wave source amplitudes W_{01} and W_{02} at different altitudes in the thermosphere. One can see amplitude ratios smaller, than the ratio 10 of amplitudes of the surface source (1), and ratios of momentum flux and wave accelerations smaller than 100 for those at the surface.

Such small ratios in Table 1 mean larger dissipation and energy transfer to the mean flow for larger AGW amplitude. Especially, this is noticeable at altitudes above 150 km, where ratios in Table 1 become smaller than one, which means that amplitudes, momentum fluxes and wave accelerations may be smaller at larger amplitude of the surface wave source. The last column in Table 1 shows larger wave-induced mean velocities at larger wave source amplitude (see also Figs. 3 and 8). At high wave source amplitude, the wave-induced mean speed may become close to the wave horizontal phase speed and near-critical layer may occur at altitudes 100–150 km, which provide strong dissipation of primary wave mode propagating upwards from the surface wave source. This dissipation in the near-critical layer may explain so small ratios in Table 1 at altitude of 150 km.

Contribution to the wave amplitude diminution may give strong reflection of upward propagating AGWs in the region of strong vertical gradient of the background temperature at altitudes 110–150 km in Fig. 1a (Walterscheid and Hickey, 2011; Yiğit and Medvedev, 2010). Temperature gradients and AGW reflection are larger at high SA (Hickey, 1987; Vadas and Fritts, 2006; Vadas, 2007; Fritts and Vadas, 2008). Thus, resulting SA influence depends on competition between AGW amplitude increase due to smaller molecular dissipation and smaller energy transfer to the wind-induced mean flow and amplitude decrease caused by larger density and stronger reflection at higher SA.

In most cases, the mean winds in the thermosphere are moderate, which may correspond to not so big amplitudes of wave sources or to not so long their coherence time intervals. However, intensive jet streams at altitudes near 100 km are sometimes observed (Larsen, 2000; Larsen et al., 2005). Breaking AGWs propagating from below may be one of the mechanisms of creation of these strong peaks of horizontal velocity in the upper atmosphere. Such strong wave-induced jet streams can create near-critical layers with high dissipation of wave energy, which are studied in current simulation.

The results of performed numerical simulation reveal that propagation conditions and parameters of AGWs propagating from the surface wave source to the thermosphere depend on changes in background temperature, density, composition and molecular viscosity and heat conduction caused by changes in solar activity. This agrees with previous studies (Hickey, 1987; Vadas and Fritts, 2006; Klausner et al., 2009; Yiğit and Medvedev, 2010). Simulations in this study shows that at smaller wave source amplitudes AGW momentum fluxes, amplitudes and wave accelerations of the mean flow at altitudes 100–150 km are slightly larger at low SA. Similar larger AGW amplitudes, wave drag and momentum flux at altitudes above 100 km during smaller SA level were obtained by Yiğit and Medvedev (2010) with a numerical model of general circulation. This can be explained by smaller mean density at fixed thermospheric altitude at small SA, while AGW amplitudes are proportional to $\rho_0^{-1/2}$ at low dissipation (e.g. Gossard and Hooke, 1975). Larger kinematic coefficients of molecular viscosity and heat conduction lead to stronger decrease of wave amplitudes and momentum fluxes at altitudes above 150 km at low SA.

At lager amplitudes of surface wave excitation, wave breaking and smaller-scale inhomogeneities appear at altitudes 100–150 km, which are stronger at low SA. Increased dissipation of breaking AGWs may produce wave-induced jet streams with velocities close to the wave horizontal phase speed. Strong AGW dissipation in near-critical layers created by the wave-induced jet streams at altitudes 110–150 km dramatically decreases wave amplitudes and momentum fluxes of the primary AGW mode propagating from the surface wave source. The wave-induced horizontal wind becomes smaller above altitude of 150 km and allows growing amplitudes of the primary wave mode partially penetrating through the near-critical layer and of secondary AGW modes, possibly generating in the wave induced jet stream. This wave amplitude grows at $z > 150$ km is larger at high SA due to smaller velocities of wave-induced mean wind and smaller molecular viscosity and heat conduction. Accelerations of the mean flow by dissipating AGWs are generally larger at low SA. This determines stronger wave-induced forcing during periods of low SA. In almost all simulated cases, velocities of the wave-induced mean flows are stronger at low SA compared to high SA.

In the present study, we considered only influence of changes in the temperature, density, molecular weight and molecular dissipation caused by changing SA on AGW propagation from the troposphere to the thermosphere. Changes in solar activity produce also changes in ion density, ion viscosity and other characteristics influencing AGW propagation in the ionosphere. Further studies and numerical simulations are required for better understanding of the influence of solar activity on AGW propagation and characteristics in the upper atmosphere. Such studies could be useful for improvements of parameterizations of AGW effects in general circulation models (e.g., Yiğit and Medvedev, 2010).

Acknowledgements

This work was partly supported by the Russian Basic Research Foundation (grant 17-05-00458), and by the Ministry of Education and Science of Russian Federation (contract 3.1127.2014/K). Data from the SPbSU resource center “Geomodel” has been used. The authors thank A. N. Gavrilov for help in improving computer code.

References

Andreassen, O., Hvidsten, O., Fritts, D., Arendt, S., 1998. Vorticity dynamics in a breaking internal gravity wave. Part 1. Initial instability evolution. J. Fluid Mech. 367, 27–46.
AtmoSym, 2016. Multi-scale atmosphere model from the Earth's surface up to 500 km. http://atmos.kantiana.ru/. (Accessed 25 February 2018).
Baker, D., Schubert, G., 2000. Convectively generated internal gravity waves in the lower atmosphere of Venus. Part II: mean wind shear and wave mean flow interaction. J. Atmos. Sci. 57, 200–215.
Djuth, F.T., Sulzer, M.P., Gonzales, S.A., Mathews, J.D., Elder, J.H., Walterscheid, R.L., 2004. A continuum of gravity waves in the Arecibo thermosphere. J. Geophys. Res. 31, L16801. https://doi.org/10.1029/2003GL019376.
Francis, S.H., 1973. Acoustic-gravity modes and large-scale traveling ionospheric disturbances of a realistic, dissipative atmosphere. J. Geophys. Res. 78, 2278–2301.
Fritts, D.C., Alexander, M.J., 2003. Gravity wave dynamics and effects in the middle atmosphere. Rev. Geophys. 41 (1), 1003,. https://doi.org/10.1029/2001RG000106.
Fritts, D.C., Garten, J.F., 1996. Wave braking and transition to turbulence in stratified shear flows. J. Atmos. Sci. 53 (8), 1057–1085.
Fritts, D.C., Vadas, S.L., 2008. Gravity wave penetration into the thermosphere: sensitivity to solar variations and mean winds. Ann. Geophys. 26, 3841–3861.
Fritts, D.C., Vadas, S.L., Wan, K., Werne, J.A., 2006. Mean and variable forcing of the middle atmosphere by gravity waves. J. Atmos. Sol. Terr. Phys. 68, 247–265.
Fritts, D.C., Wang, L., Werne, J., Lund, T., Wan, K., 2009. Gravity wave instability dynamics at high Reynolds numbers. Part II: turbulence evolution, structure, and anisotropy. J. Atmos. Sci. 66, 1149–1171.
Fritts, D.C., Franke, P.M., Wan, K., Lund, T., Werne, J., 2011. Computation of clear-air radar backscatter from numerical simulations of turbulence: 2. Backscatter moments throughout the lifecycle of a Kelvin-Helmholtz instability. J. Geophys. Res. 116, D11105. https://doi.org/10.1029/2010JD014618.
Gavrilov, N.M., 1995. Distributions of the intensity of ion temperature perturbations in the thermosphere. J. Geophys. Res. 100 (A12), 23835–23844. https://doi.org/10.1029/95JA01927.
Gavrilov, N.M., 2007. Structure of the mesoscale variability of the troposphere and stratosphere found from radio refraction measurements via CHAMP satellite. Izvestia. Atmos. Oceanic Phys. 43 (4), 451–460.
Gavrilov, N.M., Fukao, S., 1999. A comparison of seasonal variations of gravity wave intensity observed by the MU radar with a theoretical model. J. Atmos. Sci. 56, 3485–3494.
Gavrilov, N.M., Kshevetskii, S.P., 2013a. Numerical modeling of propagation of breaking nonlinear acoustic-gravity waves from the lower to the upper atmosphere. Adv. Space Res. 51 (7), 1168–1174. https://doi.org/10.1016/j.asr.2012.10.023.
Gavrilov, N.M., Kshevetskii, S.P., 2013b. A study of propagation of nonlinear acoustic-gravity waves in the middle and upper atmosphere by means of numerical modeling, Russian J. Phys. Chem. B 7 (6), 788–794. https://doi.org/10.1134/S1990793113050163.
Gavrilov, N.M., Kshevetskii, S.P., 2014a. Numerical modeling of the propagation of nonlinear acoustic-gravity waves in the middle and upper atmosphere, Izvestiya. Atmos. Ocean. Phys. 50, 66–72. https://doi.org/10.1134/S0001433813050046.

Gavrilov, N.M., Kshevetskii, S.P., 2014b. Verifications of the nonlinear numerical model and polarization relations of atmospheric acoustic-gravity waves. Geosci. Model Dev. Discuss. (GMDD) 7, 7805–7822.
Gavrilov, N.M., Kshevetskii, S.P., 2014c. Three-dimensional numerical simulation of nonlinear acoustic-gravity wave propagation from the troposphere to the thermosphere. Earth Planets Space 66, 88,. https://doi.org/10.1186/1880-5981-66-88.
Gavrilov, N.M., Kshevetskii, S.P., 2015. Dynamical and thermal effects of nonsteady nonlinear acoustic-gravity waves propagating from tropospheric sources to the upper atmosphere. Adv. Space Res. 55 https://doi.org/10.1016/j.asr.2015.01.033.
Gavrilov, N.M., Richmond, A.D., Bertin, F., Laufeuille, M., 1994. Investigation of seasonal and interannual variations of internal gravity waves in the thermosphere over Saint-Cantin. J. Geophys. Res. 99 (A4), 6297–6306. https://doi.org/10.1029/93JA03164.
Gossard, E.E., Hooke, W.H., 1975. Waves in the Atmosphere. Elsevier Sci. Publ. Co., Amsterdam-Oxford-New York.
Hickey, M.P., 1987. A theoretical comparison of internal gravity wave propagation and dissipation in high and low temperature thermospheres. In: Implications for Orbiting Spacecraft, Paper Presented at 25th Aerospace Sciences Meeting. Am. Inst. of Aeronaut. and Astronaut., Reno, Nev.
Karpov, I.V., Kshevetskii, S.P., 2014. Formation of large-scale disturbances in the upper atmosphere caused by acoustic gravity wave sources on the Earth's surface. Geomagn. Aeron. 54 (4), 553–562.
Kikoin, I.K., 1976. Tables of Physical Quantities. Atomizdat Press, Moscow, pp. 272–279.
Klausner, V., Fagundes, P.R., Sahai, Y., Wrasse, C.M., Pillat, V.G., Becker-Guedes, F., 2009. Observations of GW/TID oscillations in the F2 layer at low latitude during high and low solar activity, geomagnetic quiet and disturbed periods. J. Geophys. Res. 114, A02313. https://doi.org/10.1029/2008JA013448.
Kshevetskii, S.P., Gavrilov, N.M., 2005. Vertical propagation, breaking and effects of nonlinear gravity waves in the atmosphere. J. Atmos. Sol. Terr. Phys. 67 (11), 1014–1030. https://doi.org/10.1016/j.jastp.2005.02.013.
Larsen, M.F., 2000. A shear instability seeding mechanism for quasiperiodic radar echoes. J. Geophys. Res. 105, 24931–24940.
Larsen, M.F., Yamamoto, M., Fukao, S., Tsunoda, R.T., Saito, A., 2005. Observations of neutral winds, wind shears, and wave structure during a sporadic- E/QP event. Ann. Geophys. 23, 2369–2375 doi:1432-0576/ag/2005-23-2369.
Liu, X., Xu, J., Liu, H.-L., Ma, R., 2008. Nonlinear interactions between gravity waves with different wavelengths and diurnal tide. J. Geophys. Res. 113, D08112. https://doi.org/10.1029/2007JD009136.
Liu, X., Xu, J., Gao, H., Chen, G., 2009. Kelvin-Helmholtz billows and their effects on mean state during gravity wave propagation. Ann. Geophys. 27, 2789–2798.
Medvedev, A.S., Gavrilov, N.M., 1995. The nonlinear mechanism of gravity wave generation by meteorological motions in the atmosphere. J. Atmos. Terr. Phys. 57, 1221–1231.
Medvedev, A.S., Yiğit, E., Kuroda, T., Hartogh, P., 2013. General circulation modeling of the Martian upper atmosphere during global dust storms. J. Geophys. Res. Planets 118. https://doi.org/10.1002/jgre.20163.
Park, J., Lühr, H., Lee, C., Kim, Y.H., Jee, G., Kim, J.-H., 2014. A climatology of medium-scale gravity wave activity in the midlatitude/low-latitude daytime upper thermosphere as observed by CHAMP. J. Geophys. Res. Space Phys. 119 https://doi.org/10.1002/2013JA019705.
Picone, J.M., Hedin, A.E., Drob, D.P., Aikin, A.C., 2002. NRLMSISE-00 empirical model of the atmosphere: statistical comparisons and scientific issues. J. Geophys. Res. 107 (A12), 1468,. https://doi.org/10.1029/2002JA009430.
Richmond, A.D., 1978. Gravity wave generation, propagation, and dissipation in the thermosphere. J. Geophys. Res. 83, 4131–4145.
Townsend, A.A., 1965. Excitation of internal waves by a turbulent boundary layer. J. Fluid Mech. 22, 241–252.
Townsend, A.A., 1966. Internal waves produced by a convective layer. J. Fluid Mech. 24, 307–319.
Vadas, S.L., 2007. Horizontal and vertical propagation of gravity waves in the thermosphere from lower atmospheric and thermospheric sources. J. Geophys. Res. 112, A06305. https://doi.org/10.1029/2006JA011845.
Vadas, S.L., Fritts, D.C., 2006. Influence of solar variability on gravity wave structure and dissipation in the thermosphere from tropospheric convection. J. Geophys. Res. 111, A10S12. https://doi.org/10.1029/2005JA011510.
Walterscheid, R.L., Hickey, M.P., 2011. Group velocity and energy flux in the thermosphere: limits on the validity of group velocity in a viscous atmosphere. J. Geophys. Res. 116, D12101. https://doi.org/10.1029/2010JD014987.
Yiğit, E., Medvedev, A.S., 2009. Heating and cooling of the thermosphere by internal gravity waves. Geophys. Res. Lett. 36, L14807. https://doi.org/10.1029/2009GL038507.
Yiğit, E., Medvedev, A.S., 2010. Internal gravity waves in the thermosphere during low and high solar activity: simulation study. J. Geophys. Res. 115, A00G02. https://doi.org/10.1029/2009JA015106.
Yiğit, E., Medvedev, A.S., 2012. Gravity waves in the thermosphere during a sudden stratospheric warming. Geophys. Res. Lett. 39, L21101. https://doi.org/10.1029/2012GL053812.
Yiğit, E., Medvedev, A.S., 2015. Internal wave coupling processes in Earth's atmosphere. Adv. Space Res. 55 (4) https://doi.org/10.1016/j.asr.2014.11.020.
Yiğit, E., Medvedev, A.S., 2016. Role of gravity waves in vertical coupling during sudden stratospheric warmings. Geosci. Letts. 3, 27. https://doi.org/10.1186/s40562-016-0056-1.
Yiğit, E., Medvedev, A.S., 2017. Influence of parameterized small-scale gravity waves on the migrating diurnal tide in Earth's thermosphere. J. Geophys. Res. Space Physics 122. https://doi.org/10.1002/2017JA024089.
Yiğit, E., Aylward, A.D., Medvedev, A.S., 2008. Parameterization of the effects of vertically propagating gravity waves for thermosphere general circulation models: sensitivity study. J. Geophys. Res. 113, D19106. https://doi.org/10.1029/2008JD010135.
Yiğit, E., Medvedev, A.S., Aylward, A.D., Ridley, A.J., Harris, M.J., Moldwin, M.B., Hartogh, P., 2012a. Dynamical effects of internal gravity waves in the equinoctial thermosphere. J. Atmos. Sol. Terr. Phys. https://doi.org/10.1016/j.jastp.2011.11.014.
Yiğit, E., Ridley, A.J., Moldwin, M.B., 2012b. Importance of capturing heliospheric variability for studies of thermospheric vertical winds. J. Geophys. Res. 117, A07306. https://doi.org/10.1029/2012JA017596.
Yiğit, E., Medvedev, A.S., England, S.L., Immel, T.J., 2014. Simulated variability of the high-latitude thermosphere induced by small-scale gravity waves during a sudden stratospheric warming. J. Geophys. Res. 119 https://doi.org/10.1002/2013JA019283.
Yiğit, E., Medvedev, A.S., Hartogh, P., 2015a. Gravity waves and high-altitude CO_2 ice cloud formation in the Martian atmosphere. Geophys. Res. Lett. 42 https://doi.org/10.1002/2015GL064275.
Yiğit, E., England, S.L., Liu, G., Medvedev, A.S., Mahaffy, P.R., Kuroda, T., Jakosky, B.M., 2015b. High-altitude gravity waves in the Martian thermosphere observed by MAVEN/NGIMS and modeled by a gravity wave scheme. Geophys. Res. Lett. 42 https://doi.org/10.1002/2015GL065307.
Yu, Y., Hickey, M.P., 2007. Numerical modeling of a gravity wave packet ducted by the thermal structure of the atmosphere. J. Geophys. Res. 112, A06308 https://doi.org/10.1029/2006JA012092.
Yue, J., She, C.–J., Liu, H.–L., 2010. Large wind shears and stabilities in the mesopause region observed by Na wind-temperature lidar at midlatitude. J. Geophys. Res. https://doi.org/10.1029/2009 JA014864.